Vacuum correlators at short distances from lattice QCD

Tim Harris,[a,*] **Marco Cè,**[b] **Harvey B. Meyer,**[c,d,e] **Arianna Toniato**[c] **and Csaba Török**[c]

[a]*School of Physics and Astronomy, University of Edinburgh, EH9 3JZ, UK*

[b]*Theoretical Physics Department, CERN, CH-1211 Geneva 23, Switzerland*

[c]*PRISMA+ Cluster of Excellence & Institut für Kernphysik, Johannes Gutenberg-Universität Mainz, Saarstr. 21, 55122 Mainz, Germany*

[d]*Helmholtz Institut Mainz, Johannes Gutenberg-Universität Mainz, Saarstr. 21, 55122 Mainz, Germany*

[e]*GSI Helmholtzzentrum für Schwerionenforschung, Planckstraße 1, 64291, Darmstadt, Germany*

E-mail: tharris@ed.ac.uk

We propose a method to help control cutoff effects in the short-distance contribution to integrated correlation functions, such as the hadronic vacuum polarization (HVP), using the corresponding screening correlators computed at finite temperature. The strategy is investigated with Wilson fermions at leading order, which reveals a logarithmically-enhanced lattice artifact in the short-distance contribution, whose coefficient is determined at this order. We then perform a numerical study with $N_f = 2$ O(a)-improved Wilson fermions and a temperature $T \approx 250$ MeV, with lattice spacings down to $a \approx 0.03$ fm, which suggests good control can be achieved on the short-distance contribution to the HVP and the Adler function at large virtuality. Finally, we put forward a scheme to compute the complete HVP function at arbitrarily large virtualities using a step-scaling in the temperature.

The 38th International Symposium on Lattice Field Theory, LATTICE2021 26th-30th July, 2021
Zoom/Gather@Massachusetts Institute of Technology

---

*Speaker

1. Introduction

Correlation functions evaluated at small distances are susceptible to large cutoff effects, which are crucial to control to obtain reliable estimates for many interesting physical observables. In many contexts, such short-distance contributions arise naturally when correlators, such as that of the electromagnetic current,

$$G(x_0) = - \int d^3x \, \langle J_1(x) J_1(0) \rangle, \qquad J_\mu = \sum_f Q_f \bar{\psi}_f \gamma_\mu \psi_f, \qquad (1)$$

are integrated over all separations x_0 with a known weight function. Examples are given by the short-distance HVP contribution to the lepton anomalous magnetic moment,

$$I(t) = \int_0^t dx_0 \, x_0^4 G(x_0), \qquad (2)$$

(which to a good approximation is independent of the lepton mass for small enough t), or the Adler function at large virtualities

$$D(Q^2) = \frac{12\pi^2}{Q^2} \int_0^\infty dx_0 [2 - 2\cos(Qx_0) - Qx_0 \sin(Qx_0)] G(x_0). \qquad (3)$$

The integrands of these quantities are shown in figure 1 on the lattice with $N_f = 2$ Wilson fermions as described in section 3, which illustrates they are dominated by the region around $x_0 \sim 0.2$ fm for the choices $t \sim 0.2$ fm and $Q \sim 2.4$ GeV. In the following we concentrate on the first observable, the short-distance HVP contribution to the lepton magnetic moment or truncated fourth moment of the correlator, but the full results for the Adler can be found in ref. [1].

Power-counting suggests that the cutoff effects for the lattice correlator $\mathcal{G}$ are enhanced at small distances [2], where, in the massless limit and for $x_0 \Lambda \ll 1$, the only relevant scale is given by the distance x_0, and we have

$$\mathcal{G}(x_0, a) = G(x_0) + \text{const.} (a/x_0)^2 G(x_0) + \ldots, \qquad (4)$$

assuming full O(a)-improvement and ignoring the dependence of the running coupling on the cutoff scale. As we show in the following section, this enhancement of the cutoff effects in the correlation function leads to a logarithmic enhancement of the leading a^2 discretization effects in the short-distance HVP contribution to the lepton magnetic moment already at leading order with free fermions.

Thermal improvement Due to the breakdown of the Symanzik effective theory at short distances, it is desirable to seek an alternative approach to control cutoff effects in integrated correlation functions. In the following, we make use of the screening correlator analogous to eq. (1)

$$G^{\text{th}}(x_3) = - \int dx_0 dx_1 dx_2 \, \langle J_1(x) J_1(0) \rangle_T \qquad (5)$$

evaluated at temperature T, in a $T^{-1} \times L^3$ volume. Compared with a vacuum ensemble of dimensions $L_0 \times L^3$, the screening correlator is relatively cheap to compute, as the volume is a factor $L_0 T$ smaller
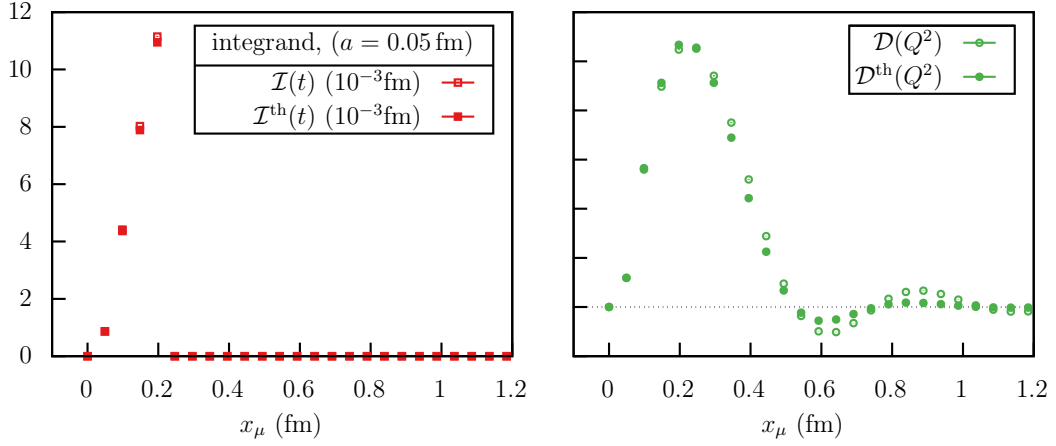
Figure 1: The integrand of the fourth moment truncated at $t \sim 0.2$ fm (left) and the Adler function with $Q \sim 2.4$ GeV (right) at finite lattice spacing $a \sim 0.05$ fm. The integrals are dominated by the contributions around $x_0 \sim 0.2$ fm. The filled symbols depict the thermal observable, while the open symbols represent the corresponding vacuum contribution.

and one can reach smaller lattice spacings at a fixed cost, which is illustrated in figure 2. One can define the thermal analogues of the integrated quantities, such as the fourth moment I^{th}, by utilizing this screening quantity. The operator-product expansion predicts that the leading x_0^{-3} singularity of the correlators cancels when the thermal quantity is subtracted, so that the relative difference in the integrated observable is strongly suppressed with tT

$$\frac{I(t) - I^{\text{th}}(t)}{I(t)} = \text{O}((tT)^3). \tag{6}$$

Likewise, while the artifacts on the lattice estimator $\mathcal{I}$ are $\text{O}(a^2)$ up to logarithms in the $\text{O}(a)$-improved theory, the artifacts on the difference are also parametrically suppressed by $(tT)^3$. This suggests writing a lattice estimator using the decomposition

$$\widehat{\mathcal{I}}(t) = \underbrace{\mathcal{I}^{\text{th}}}_{\text{O}(a_{\text{th}}^2) \text{ artifacts}} + \underbrace{[\mathcal{I} - \mathcal{I}^{\text{th}}]}_{\text{O}(a^2(tT)^3) \text{ artifacts}}, \tag{7}$$

where the first term on the right-hand side can be estimated using the thermal simulations down to small lattice spacings a_{th}, while the remainder which depends on the costly vacuum ensembles can be estimated using coarser lattices. In particular, the size of the artifacts on the correction will be parametrically smaller as long as the ratio of lattice spacings between the thermal and vacuum lattices a_{th}/a does not fall below $\sqrt{(tT)^3}$.

2. Leading-order perturbative study

In order to investigate the strategy, we computed the isovector vector correlator at leading order in perturbation theory with $N_{\text{f}} = 2$ massless Wilson fermions, using one local and one conserved current. We expect the leading-order perturbative computation to capture the gross features of the
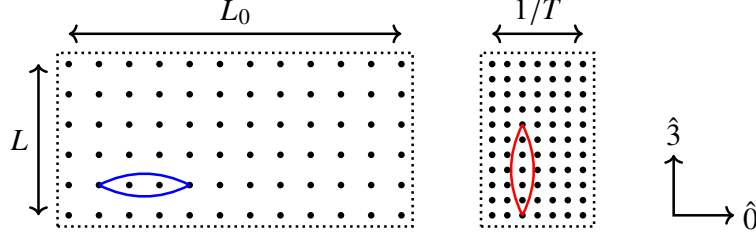
Figure 2: Illustration of the geometry of the vacuum lattices (left) and thermal lattices (right) with smaller temporal size but finer lattice spacing. Note also the correlators in the thermal ensemble are computed in the orthogonal screening direction.

t (fm)	$\|c_0 - I^{\text{th}}(t)\|/I^{\text{th}}(t)$		Ansatz
0.2	2%	0.9%	$c_0 + c_2 a^2$
	2%	0.2 %	$c_0 + c_2 a^2 + c_4 a^4$
0.4	0.8%	0.06 %	$c_0 + c_2 a^2$
	0.4%	< 0.01%	$c_0 + c_2 a^2 + c_4 a^4$
	plain	subtr.	

t (fm)	$\|c_0 - I(t)\|/I(t)$	
0.2	2%	0.2%
0.4	1%	0.04 %
	$\mathcal{I}$	$\hat{\mathcal{I}}$

Table 1: The relative accuracy of the continuum limit in the leading-order case for the thermal observable (left) and the vacuum observable (right) using realistic lattice sizes and continuum extrapolations. In the thermal case, either linear or quadratic fits in a^2 were used, with ("subtr.") or without ("plain") the subtraction of the logarithmic term. For the vacuum fits, the observable with and without the thermal subtraction is given.

strategy given the short-distance nature of the observable. In addition to providing a cross-check of the operator-product expansion at leading order, this enabled a explicit computation of the lattice artifacts.

Logarithmic enhancement of lattice artifacts The singular behaviour of the lattice artifacts observed in eq. (4) induces a logarithmic enhancement of the leading $O(a^2)$ lattice artifacts even at leading order in perturbation theory. This does not depend on the specific details of the lattice discretization. For $N_{\text{f}} = 2$ Wilson fermions, and the isovector correlator with $Q_{\text{u}} = -Q_{\text{d}} = \frac{1}{\sqrt{2}}$, we find from an explicit computation that

$$\mathcal{I} = I + c_{\mathcal{I}} a^2 \log(1/a) + O(a^2), \tag{8}$$

$$c_{\mathcal{I}} = \frac{7 N_{\text{c}}}{60 \pi^2}, \tag{9}$$

with a similar expression for the Adler function. The leading-order logarithm observed here may be particularly severe as it appears with the positive unit power, in constrast to the next-to-leading order logarithms due to the dependence of the running coupling on the cutoff scale [3]. This enhancement, which is present in both the thermal and vacuum quantities, illustrates the delicate nature of the continuum limit.
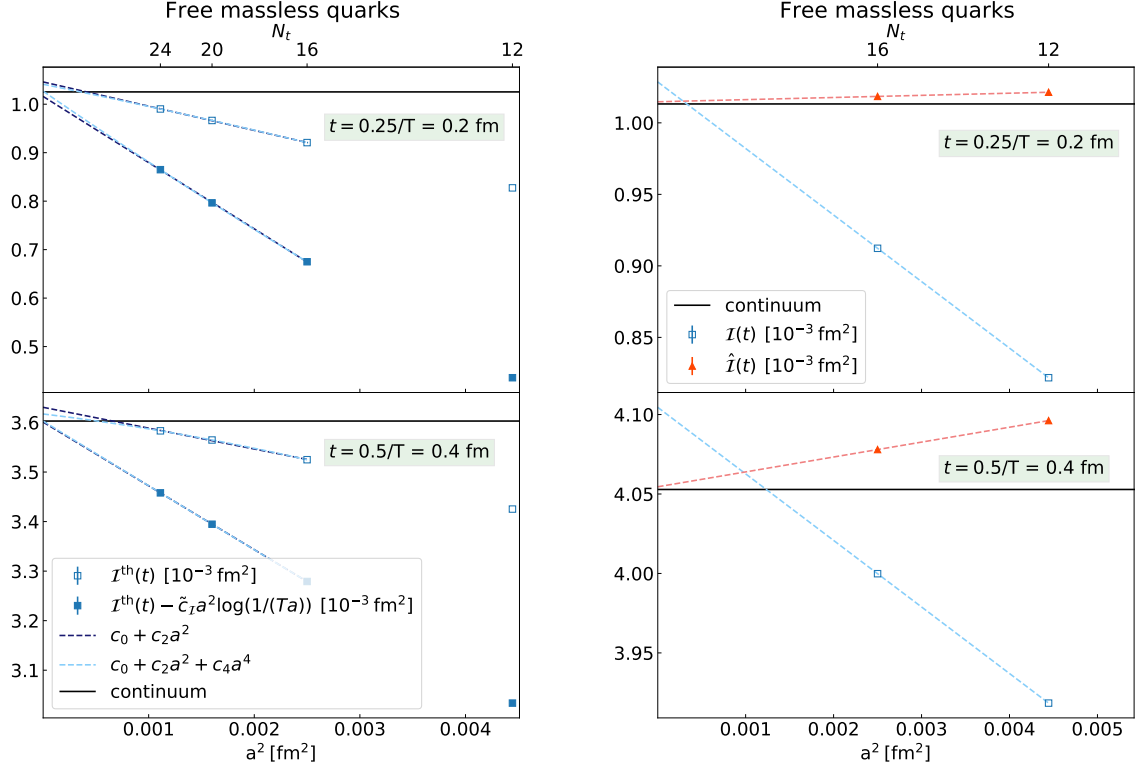
Figure 3: The continuum limit of the thermal observable (left) and vacuum observable (right). The top and bottom panels correspond to $tT = 0.25$ and $tT = 0.5$ respectively. For the thermal case, two Ansätze are illustrated, and the data with and without the subtraction of the logarithmic artifact with the filled and open symbols respectively. In the vacuum case, the observable with (without) thermal subtraction is shown with red (blue) points.

To investigate the strategy of improvement, we computed the thermal lattice observable with realistic thermal lattice sizes of $1/aT = 12, 16, 20, 24$, and the thermal to vacuum correction using only coarser lattice sizes with $1/aT = 12, 16$ in the thermal case.[1] For the thermal observable (left panel), the approach to the known continuum limit is improved for both cases $tT = 0.25$ (top) and $tT = 0.5$ (bottom) if the known logarithmic term is subtracted, which can be examined in detail in table 1. For the vacuum case, the parametric reduction in the lattice artifacts explained in the introduction is observed between the improved (red) and the unimproved data (blue). Without the thermal subtraction, an overestimate of this contribution is observed at the per-cent level, whereas the case utilising the thermal subtraction reaches easily sub-percent precision.

---

[1]These lattice sizes correspond to the state-of-the-art in non-perturbative simulations. Indeed, if the scale is set by the temperature to $T \approx 250\,\text{MeV}$ as we take as a reasonable choice later, then the smallest lattice spacing for the vacuum computation correponds to $a \sim 0.05\,\text{fm}$ and $0.03\,\text{fm}$ for the thermal ones.

	L/a	$1/aT$	L_0/a	a (fm)	$6/g_0^2$	N_{conf}
F7	48	12	96	0.0658	5.3	482
O7	64	16	128	0.049	5.5	305
W7	80	20	–	0.039	5.685 727	1566
X7	96	24	–	0.033	5.827 16	511

Table 2: The lattice parameters for the numerical study with $N_{\mathrm{f}} = 2$ O(a)-improved Wilson fermions. The vacuum ensembles are from the CLS collaboration and the tuning to the line of constant physics for the fine thermal ensembles was performed in ref. [4]. The pseudoscalar mass in the vacuum is approximately $m_\pi \approx 270$ MeV and the temperature is $T = 254$ MeV. Note the large lattice sizes and small lattices spacings available for the thermal case.

3. Numerical results with $N_{\mathrm{f}} = 2$ Wilson fermions

Given the encouraging results from the leading-order theory, we investigated the improvement strategy with $N_{\mathrm{f}} = 2$ non-perturbatively O(a)-improved Wilson fermions in the sea. Details of the ensembles used to compute the thermal observable with lattice spacings down to $a_{\mathrm{th}} \sim 0.03$ fm, and down to $a \sim 0.05$ fm for the vacuum case. The line of constant physics set by the quark mass and L is fixed going toward the continuum limit in both the vacuum and thermal cases. Although the current is not on-shell O(a)-improved, we expect, due to the lack of chiral-symmetry breaking at short distances (and high temperatures [5]), that the O(a) cutoff effects will be suppressed and proportional to the quark mass, given that off-shell contributions contribute at higher order. We use the results of the previous section to also implement the subtraction of the lattice artifacts at leading order in perturbation theory for the thermal observable according to

$$\mathring{\mathcal{I}}^{\mathrm{th}}(t, a) = \mathcal{I}^{\mathrm{th}}(t, a) - \left[\mathcal{I}^{\mathrm{th}}(t, a) - I^{\mathrm{th}}(t) \right]_{\mathrm{LO}}. \tag{10}$$

In figure 4 (left), the addition of the two fine lattices for the thermal observable clearly improves the robustness of the continuum limit, for $t = 0.1974$ fm. We use a systematic error from half of the difference between the two extrapolations depicted in the figure, which are explained in the caption. The subtraction of the leading-order lattice artifacts (blue) is beneficial in removing a large fraction of the lattice artifacts in the thermal observable. For the vacuum observable, the lattice artifacts which remain after subtracting the thermal component (orange) are significantly smaller, as was observed in the leading-order computation. In contrast to the unimproved data (green), the resulting extrapolation is under much better control and a much smaller estimate of the corresponding systematic error is obtained.

For illustration, a final result can be obtained by combining the thermal observable with the subtraction of leading-order lattice artifacts and the mean of the linear and quadratic extrapolations for the remainder

$$I(t = 0.1974 \, \mathrm{fm}) = 1.035(9)_{\mathrm{stat}}(19)_{\mathrm{cont}} \times 10^{-3} \mathrm{fm}^2, \tag{11}$$

while the systematics are added in quadrature. We find satisfactory agreement (within the un-accounted mass and non-perturbative effects) with the result from perturbation theory using the
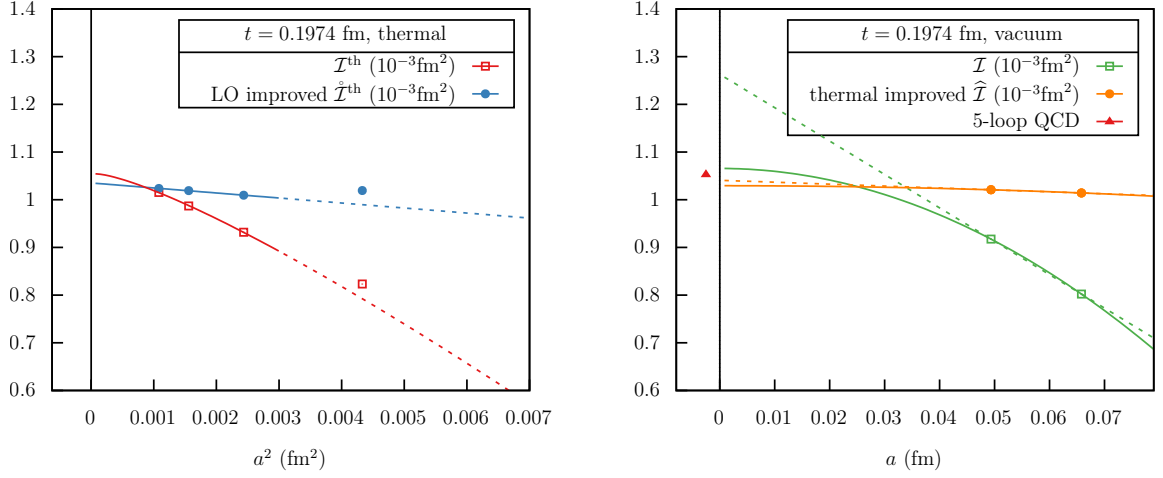
6

Figure 4: The continuum limit for the thermal (left) and vacuum (right) observable with $N_f = 2$ O(a)-improved Wilson fermions. In the thermal case (red), the Ansatz is quadratic in a including the leading-order logarithmic artifact, while for the leading-order improved observable (blue) it is linear in a^2. In the vacuum, the case with (without) thermal subtraction is shown in orange (green). Ansätze linear in a (dashed) and in a^2 (solid) are shown in both cases in the vacuum.

known five-loop spectral density, from which we obtain $I_{\text{pert}}(t = 0.1974\,\text{fm}) = 1.059^1_{-6} \times 10^{-3}\text{fm}^2$, where the asymmetric errors are due to the uncertainty in the $N_f = 2$ $\Lambda_{\overline{\text{MS}}}$.

4. The (discrete) Adler function at any scale

The analysis of the temperature effects on the short-distance current correlator leads to a practical strategy for computing non-perturbatively the Adler function, or its discrete analogue $\Delta_2(Q^2) = \Pi(Q^2) - \Pi(Q^2/4)$, at arbitrarily high energies Q^2 while keeping cutoff effects under control. The preceding analysis suggests that in fact a good precision at the percent level can be obtained in a single-scale simulation for the thermal analogue of $\Delta_2(Q^2)$ with $T = Q/8\pi$. It is seemingly impossible to satisfy simultaneously the conditions

$$T \lesssim \Lambda \qquad \text{and} \qquad Q \ll a^{-1} \tag{12}$$

for arbitrarily large Q to obtain a vacuum estimate. However, for large Q^2, the temperature effects are known to be of order $(\pi T/Q)^4$, which suggests that an accurate estimate of the vacuum correction would be obtained by including the difference to $T/2$ as

$$\Delta_2(Q^2) \approx \Delta_2(Q^2; T) - [\Delta_2(Q^2; T) - \Delta_2(Q^2; T/2)]. \tag{13}$$

In this case only the double hierarchy

$$T \ll Q \ll a^{-1} \tag{14}$$

needs to be satisfied as the vacuum scale has been removed and the temperature T has been linked to the scale Q. This allows any range of energies to be explored with this given level of precision. This strategy has also been validated at leading order in perturbation theory [1], where indeed the omitted correction from $T/2$ to the vacuum was observed to be a relative effect at the per-mille level. In the Schwinger model a related strategy has also been presented at this conference [6].

5. Conclusions

The study of the temperature effects on the short-distance electromagnetic current correlator has led to new insights to control the cutoff effects on vacuum quantities like the Adler function at large energies, or the short-distance HVP contribution to the muon anomalous magnetic moment. These effects were investigated using the operator-product expansion at finite temperature which has also been worked out at next-to-leading order [7]. A full computation of the lattice correlator at leading order in perturbation theory with massless Wilson fermions allowed the asymptotics to be cross-checked, and to study the proposal to use a thermal subtraction to improve the continuum limit. A resulting observation was that, for any discretization, a logarithmically-enhanced $O(a^2)$ lattice artifact is present in these observables, which highlights that the continuum limit must be taken with care. The strategy was implemented for $N_{\mathrm{f}} = 2$ non-perturbatively $O(a)$-improved Wilson fermions for the HVP contribution to muon anomaly up to $x_0 \approx 0.2\,\mathrm{fm}$ and utilizing a thermal ensemble with a temperature of $T \approx 250\,\mathrm{MeV}$. The use of the thermal subtraction gave a clear advantage, while the subtraction of the leading-order lattice artifacts was beneficial where small lattice spacings were available. Finally, a step-scaling strategy was outlined to compute a discrete analogue of the Adler function at arbitrarily large energies, which is relevant to determine the hadronic contribution to the running of the electromagnetic coupling at the Z-pole.

Acknowledgments

References

[1]   M. Cè et al. In: (June 2021). arXiv: 2106.15293 [hep-lat].

[2]   M. Della Morte et al. In: *Phys. Lett. B* 672 (2009), pp. 407–412. arXiv: 0807.1120 [hep-lat].

[3]   N. Husung et al. In: *Eur. Phys. J. C* 80.3 (2020), p. 200. arXiv: 1912.08498 [hep-lat].

[4]   A. Steinberg. PhD thesis. Mainz U., 2021.

[5]   M. Dalla Brida et al. In: *JHEP* 04 (2020), p. 043. arXiv: 2002.06897 [hep-lat].

[6]   F. Frech et al. In: *PoS* LATTICE2021 (to appear), p. 218.

[7]   M. Cè et al. In: *JHEP* 03 (2021), p. 035. arXiv: 2012.07522 [hep-ph].

[8]   Jülich Supercomputing Centre. In: *Journal of large-scale research facilities* 5.A135 (2019). URL: http://dx.doi.org/10.17815/jlsrf-5-171.

[9]   R. G. Edwards and B. Joo. In: *Nucl. Phys. B Proc. Suppl.* 140 (2005). Ed. by G. T. Bodwin et al., p. 832. arXiv: hep-lat/0409003.

[10] M. Lüscher and S. Schaefer. In: *Comput. Phys. Commun.* 184 (2013), pp. 519–528. arXiv: 1206.2809 [hep-lat].